ISIJ International, Vol. 40 (2000), No. 2, pp. 207–210

Stress Rupture Ductility Diagram—A Diagnostic Tool

Satyabrata CHAUDHURI, Nilima ROY and Rabindra Nath GHOSH

National Metallurgical Laboratory, Council of Scientific and Industrial Research, Jamshedpur 831007, India.
E-mail: sc1@csnml.ren.nic.in

(*Received on August 27, 1999; accepted in final form on October 19, 1999*)

The present work suggests a methodology for construction of stress rupture ductility diagram using the concept of geometrical factor k that determines the nature of creep rupture. Large volumes of stress rupture ductility data of a range of engineering materials generated experimentally in the laboratory and reported in the literature have been used to study the nature of creep rupture by superimposition of these data on the above diagram.

The rupture ductility of Ni-base superalloy, when superimposed on such diagram, indicates that the failure in this alloy could be due to limited amount of localised deformation or cavitation. In case of Zr–Nb alloy, the rupture ductility data lie in the necking regime extending from k=0.9 to 0.4. In contrast, the data on Cr–Mo steel show a wider variation extending from the regime of cavitation to extensive necking.

Reliable prediction of rupture ductility is possible within a narrow range of k in which the nature of creep rupture remains the same.

KEY WORDS: stress rupture ductility diagram; Cr–Mo steel; Zr–Nb alloy; Ni-base superalloy; elongation; reduction in area; geometrical factor; cavitation; necking; intergranular fracture; transgranular fracture; Scanning Electron Microscope.

1. Introduction

Prediction of stress rupture ductility of engineering materials is of considerable importance for integrity assessment of high temperature components. The presence of localised defects and stress concentration often plays critical roles during creep leading to rupture. In such situations, growth of cracks and defects would be governed by the stress rupture ductility of the material.[1] Since in many cases it varies with rupture strength, the properties must be optimised for a given application.

Stress rupture tests are commonly used to predict long-term rupture strength of high temperature materials. Though the percentage elongation and reduction in area of the test specimens have been reported,[2–8] these have not been widely used for prediction of long term rupture ductility. This is primarily because both reduction in area and elongation do not show a definite trend with stress and temperature. The total rupture elongation of the test specimen consists of two distinct parts *viz*. uniform deformation and localised deformation. The extent of uniform deformation beyond which necking *i.e*. localised deformation sets in may change with testing conditions. This, therefore, makes reliable prediction of rupture ductility a difficult task.

A rigorous analysis of conditions under which necking sets in during creep is not reported in literature. However, approximate analyses due to Hart[9] as well as Burke *et al*.[10] gives a fairly complete picture. Their analysis shows that under Newtonian viscous flow, the stress exponent being unity, necking never sets in. However most engineering materials have significantly higher creep stress exponent (n). Therefore necking may set in quite early, for which a detected level of necking, typically a creep strain of about 5 to 10% may be necessary. Analysis of Burke and Nix[10] shows that the strain (ε_n) at which necking first influences creep rate is given by:

$$\varepsilon_n = 2/(n-1) \quad \text{.....(1)}$$

This indicates that in case of 2.25Cr–1Mo steel, where n is reported to be around 11,[11] necking sets in when creep strain (ε_n) is 0.2, which is rather high. Therefore, a better analytical method to understand and describe the nature of localised deformation during creep is highly essential.

In this paper, a simple method for construction of stress rupture ductility diagram is suggested. This can be used as a diagnostic tool which would at a first glance provide a quantitative estimate of the extent of localised deformation or uniformly distributed void growth in a given test condition.

2. Construction of Stress Rupture Ductility Diagram

Over the years, large volumes of stress rupture data have been generated experimentally in the laboratory for a wide range of materials primarily from constant load uniaxial stress rupture tests. Besides reporting the time to rupture as a function of stress and temperature, the rupture strain at failure are also reported in terms of both reduction in area (RA) and elongation (EL). These are calculated from the length (l) and cross sectional area (A) of the test specimen

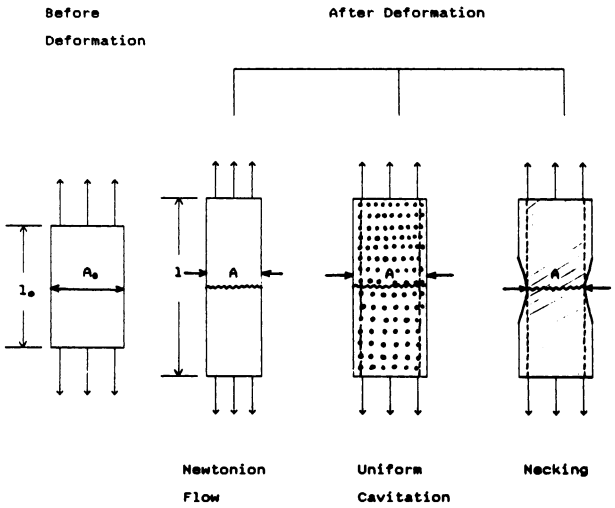

Fig. 1. Schematic representation of the nature of creep deformation.

at rupture using the following expressions:

$$RA=(1-A/A_o) \quad \text{.....(2)}$$

$$El=(l/l_o)-1 \quad \text{.....(3)}$$

Where A_o and l_o represent the original cross section and gauge length of the test specimen respectively.

Whilst the product $A_o l_o$ represents the initial volume of the test specimen, the product Al at rupture may have a totally different physical significance depending on the nature of creep deformation. This is evident from the schematic representation of the nature of creep deformation given in **Fig. 1**. Under ideal Newtonian flow, deformation is uniform all along the gauge length. This implies that the product Al would still represent the volume of the test specimen. Since deformation is not accompanied by any change in volume, the $Al/A_o l_o$ will be unity.

On the other hand, if such a deformation is accompanied by nucleation and growth of voids as is found in a number of high temperature materials, the product Al would exceed the original volume by the volume fraction of cavities. Therefore, in such a situation, the ratio $Al/A_o l_o$ should be greater than unity.

Most rupture in uniaxial tensile creep test is preceded by localised deformation as schematically shown in Fig. 1. Since in this case A denotes the cross section area at the necked region, the product Al would therefore represent only a part of the original volume. Consequently, the ratio $Al/A_o l_o$ is expected to be less than unity. Indeed its magnitude could give an indication of the severity of necking. On the whole, therefore, the ratio $Al/A_o l_o$, which is hereafter designated as k, is a simple indicator of the nature of creep rupture. The magnitude of k will depend on the material as well as test condition. Assuming k to be a factor determining the nature of creep rupture, it is possible to derive the following relationship between RA and EL using Eqs. (2) and (3)

$$RA=1-k/(1+EL) \quad \text{.....(4)}$$

Thus plotting reduction in area against elongation for various values of k, a stress rupture ductility diagram could be generated as shown in **Fig. 2**. The stress rupture ductility data for a range of materials are superimposed on the diagram to understand the nature of rupture. The line corresponding to $k=1$ represents ideal Newtonian deformation and it divides the space into two distinct regions dominated by varying degrees of either necking or cavitation.

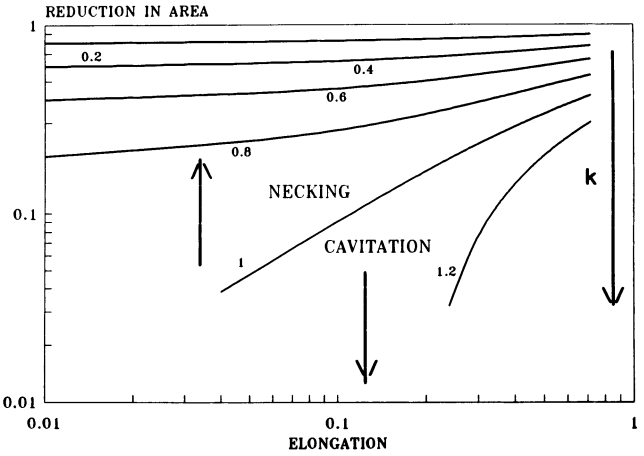

Fig. 2. Stress rupture ductility diagram.

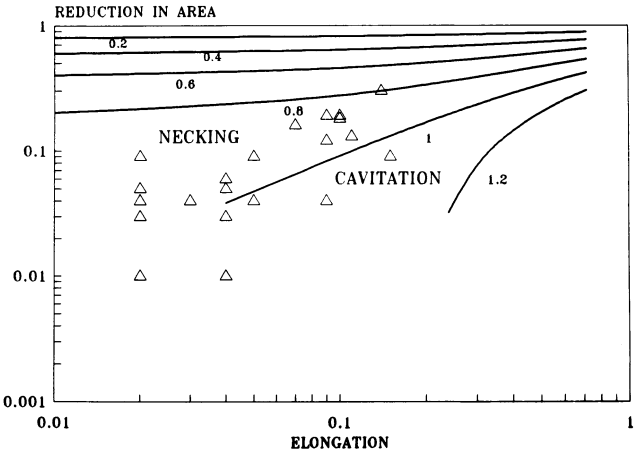

Fig. 3. Rupture ductility data of Ni-base superalloy.

3. Results and Discussion

The stress rupture ductility data of a range of engineering materials such as Cr–Mo steel,[4] Zr–Nb alloy,[6] Ni-base superalloy,[12] when superimposed on the above ductility diagram, show a definite trend in spite of wide scatter. In case of Ni-base superalloy, the regime of available data, as shown in **Fig. 3**, is scattered on either side of the curve representing $k=1$, *i.e.* corresponding to Newtonian flow. This indicates that failure in this alloy could be due to only a limited amount of either localised deformation or cavitation depending on the test parameter. Indeed cavitation has been reported to be a dominant mode of failure in these alloys and necking is not extensive.[13]

In the case of Zr–Nb alloy, all test data, as shown in **Fig. 4**, are in the necking regime extending from $k=0.9$ to $k=0.4$. The data on Cr–Mo steel, as shown in **Fig. 5**, however show a much wider variation; extending from the regime of cavitation to extensive necking with k approaching 0.1. **Figures 6–8** show the plots of rupture elongation as a func-

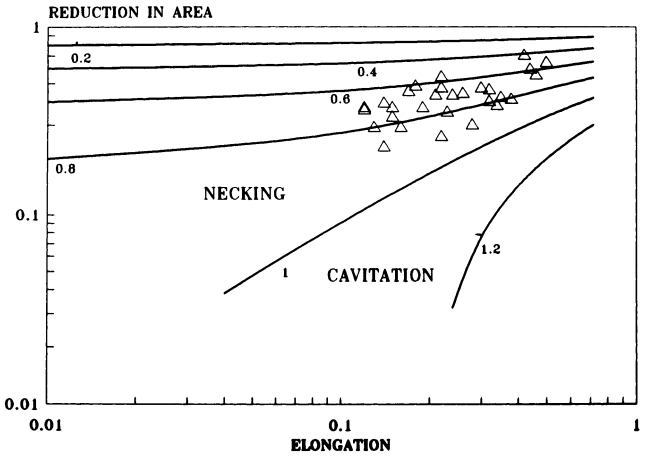

Fig. 4. Rupture ductility data of Zr–2.5%Nb alloy.

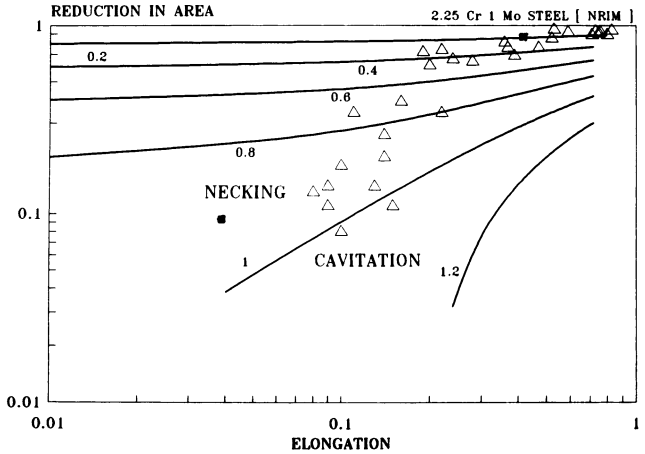

Fig. 5. Rupture ductility data of 2.25Cr–1Mo steel. [■ represents ductility data as referred in Fig. 9 and Fig. 10.]

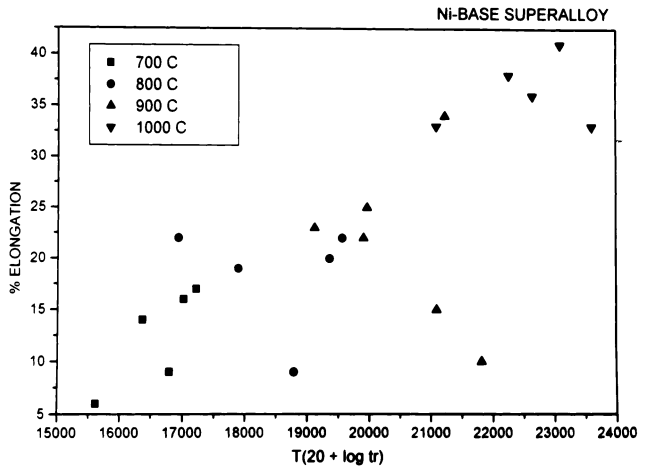

Fig. 6. Rupture elongation of Ni-base superalloy as a function of Larson–Miller-Parameter.

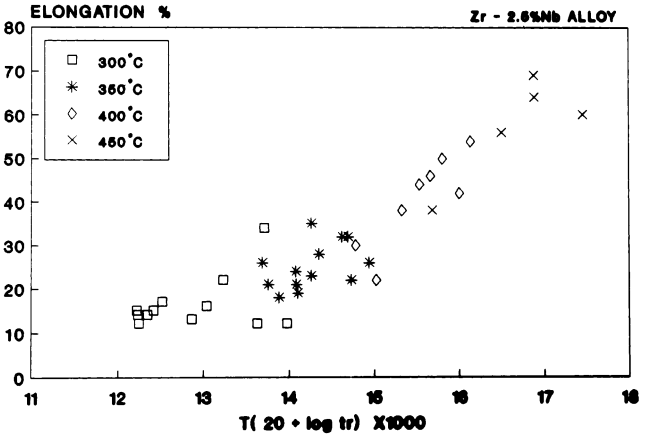

Fig. 7. Rupture elongation of Zr–2.5%Nb alloy as a function of Larson–Miller-Parameter.

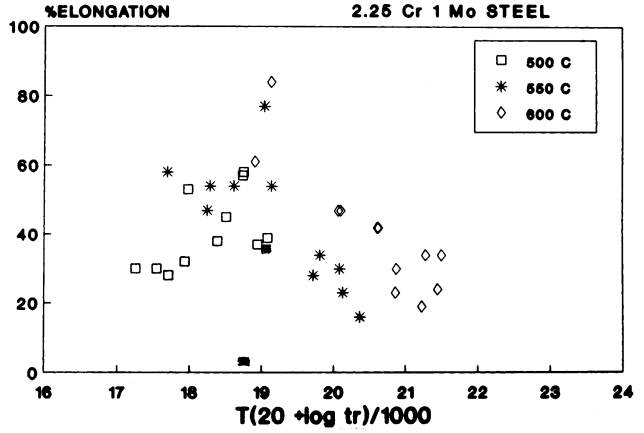

Fig. 8. Rupture elongation of 2.25Cr–1Mo steel as a function of Larson–Miller-Parameter. [■ represents rupture elongation (EL) as referred in Fig. 9 and Fig. 10.]

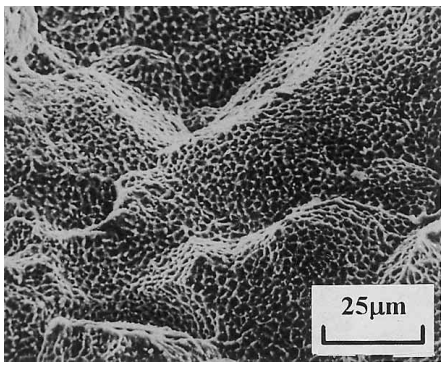

Fig. 9. Intergranular fracture in creep exposed 2.25Cr–1Mo steel specimen. [Typical ductility values are EL=3.7%, RA= 9.3%.]

tion of Larson–Miller Parameter (LMP) for the three alloys considered in this work. Whilst data on Ni-based superalloy (Fig. 3) and Zr–Nb alloy (Fig. 4) show a definite trend, there is no definite correlation in case of Cr–Mo steel (Fig. 5). This is obvious because the geometrical factor k varies widely in case of steel unlike the other two alloys.

Examination of the fractured surface of the creep exposed specimen of Cr–Mo steel using Scanning Electron Microscope, as shown in **Fig. 9**, indicates predominantly intergranular fracture. The geometrical factor k for this specimen as estimated from Eq. (4) is 0.94. This is characteristic of most intergranular rupture where necking is not extensive. In contrast to this, **Fig. 10** shows that for lower values of k (=0.23) the mechanism of creep rupture is predominantly transgranular, the necking or localised deformation being highly predominant. Therefore in order to develop an appropriate method for prediction of long term rupture ductility, geometrical factor k must be taken into consideration.

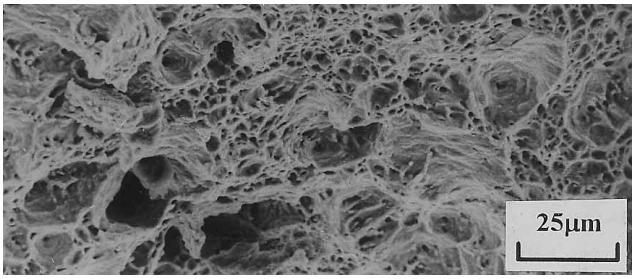

Fig. 10. Transgranular fracture in creep exposed 2.25Cr–1Mo steel specimen. [Typical ductility values are EL=38%, RA=83%.]

Clearly further work needs to be done along this direction.

The construction of the ductility diagram, however, is based on the assumption that both necking and void growth may not take place simultaneously. This may not be so particularly at values of k close to unity. Therefore, construction of the diagram in this regime may require further refinement. However, the test data in most cases lie well in the regime of prominent necking, signifying utility of such plot in estimating the influence of test parameter on k, the geometrical factor, and help understand why in certain alloys prediction of rupture ductility becomes difficult.

4. Conclusions

The concept of geometrical factor k is introduced to construct stress rupture ductility diagram. Superimposition of rupture ductility data both in terms of elongation and reduction in area on this diagram helps in estimating the magnitude of k as well as predicting the nature of creep rupture. Reliable prediction of rupture ductility is possible within a narrow range of k in which the nature of creep rupture remains the same.

Acknowledgements

The authors are grateful to Prof. P. Ramachandra Rao. Director, National Metallurgical Laboratory for his kind permission to publish this paper. They wish to thank Mr. Patange Siva Subba Rao for his help in the preparation of the manuscript of this paper.

REFERENCES

1) R. Viswanathan: Damage Mechanisms and Life Assessment of High Temperature Components, ASM International, Metals Park, Ohio, (1989), 79.
2) Data sheets on the elevated temperature properties of normalised and tempered 2.25Cr–1Mo steel for boiler and pressure vessels, NRIM Creep data sheet, No. 11B, (1997).
3) H. Wolf: Kriechen der Legierungen NiCr22Co12Mo und 10CrMo910 bei Konstanter und Zyklischer Beanspruchung, D. Ing. Thesis, Erlangen University, Erlangen, (1990).
4) S. Chaudhuri, R. Singh and R. N. Ghosh: Stress Rupture Properties of Indigenously Produced 2.25Cr–1Mo Steel, NML Report No. 1205, (1985).
5) M. P. Mishra, H. U. Borgstedt, M. D. Mathew, S. L. Mannan and P Rodriguez: *Int. J. Pressure Vessels Piping*, **72** (1997), 111.
6) S. Chaudhuri, R. K. Sinha, R. Singh, R. N. Ghosh, T. K. Sinha and S. Banerjee: Creep Behaviour of Zr–2.5%Nb Pressure Tube Materials, Proceedings, International Conference on advances in Physical Metallurgy, ed. by S. Banerjee and R.V. Ramanujan, Gordon and Breach Publishers, Bombay, (1996), 447.
7) A. K. Ray, Y. N. Tiwary, A. N. Sinha, R. K. Sinha, R. Singh and S. Chaudhuri: *Engineering Failure Analysis*, **5** (1998), 289.
8) Data sheets on the elevated temperature properties of 9Cr–2Mo steel tube for power boiler and 9Cr–2Mo steel plate for power plant, NRIM Creep data sheet No. 46, (1998).
9) E. W. Hart: *Acta Metall*, **15** (1967), 351.
10) M. A. Burke and W. D. Nix: *Acta Metall*, **23** (1975), 793.
11) S. Chaudhuri, N. Roy and R. N. Ghosh: Influence of Microstructures on Creep Behaviour of 2.25Cr–1Mo Steel, NML Report No. 11420131, (1990).
12) Data sheets on the elevated temperature properties of Nickel based 19Cr–18Co–4Mo–3Ti–3Al–B Superalloy castings and forgings for gas turbine blades, NRIM data sheet No. 34A, (1989).
13) B. F. Dyson and T. B. Gibbons: *Acta Metall. Mater.*, **35** (1987), 2355.